Nano Research

ISSN 1998-0124 CN 11-5974/O4
https://doi.org/10.1007/s12274-021-3491-z

Research Article

SiO_x/C-Ag nanosheets derived from Zintl phase $CaSi_2$ via a facile redox reaction for high performance lithium storage

Jie Xie[1,2], Lin Sun[1,2,3] (✉), Yanxiu Liu[2], Xinguo Xi[2], Ruoyu Chen[1] (✉), and Zhong Jin[3] (✉)

[1] *Jiangsu Province Cultivation Base for State Key Laboratory of Photovoltaic Science and Technology, School of Petrochemical Engineering, Changzhou University, Changzhou 213164, China*
[2] *School of Chemistry and Chemical Engineering, Yancheng Institute of Technology, Yancheng 224051, China*
[3] *Key Laboratory of Mesoscopic Chmistry of Ministry of Education (MOE), School of Chemistry and Chemical Engineering, Nanjing University, Nanjing 210023, China*

Received: 2 February 2021 / **Revised:** 1 April 2021 / **Accepted:** 1 April 2021

ABSTRACT

As one of the high-capacity anodes in lithium-ion batteries (LIBs), silicon oxide (SiO_x) has attracted wide attention due to its high theoretical capacity, low cost, and proper working voltage. However, the huge volume change and the intrinsic poor conductivity of SiO_x still hinder the practical applications. How to address the issues is the focus of current research. In this work, firstly, hydrogen passivated Si nanosheets (Si_6H_6) were prepared from Zintl phase $CaSi_2$, then, two-dimensional Ag nanoparticle modified SiO_x/C nanocomposite was prepared via a facile complex redox reaction between Si_6H_6 and $AgNO_3$-aniline complexing agent. In this design, aniline was served as carbon sources, and Si_6H_6 could be transformed to SiO_x by $AgNO_3$ in mild solution condition. The obtained Ag modified SiO_x/C (SiO_x/C-Ag) electrode exhibited high specific capacity (550 $mAh \cdot g^{-1}$ at 0.6 $A \cdot g^{-1}$), superior rate, and cycling performance when served as anode for LIBs.

KEYWORDS

SiO_x, anode, LIBs, redox reaction, two-dimensional structure, solution synthesis

1 Introduction

As widely used rechargeable batteries, lithium-ion batteries (LIBs) endow the advantages of high specific capacity, low self-discharge, no memory effect, and superior cycle stability compared with traditional secondary batteries [1]. However, for the anode material of LIBs, the current commercial graphite anode cannot meet the market requirement of high energy density [2]. Recently, compared with pure silicon (Si), much attention have been payed to silicon oxides (SiO_x), which features with high theoretical capacity (1,965 $mAh \cdot g^{-1}$ for SiO_2, 2,680 $mAh \cdot g^{-1}$ for SiO), suitable working potential, non-toxicity, and prolonged lifespan [3–5]. Especially, the *in-situ* generated lithium silicates (such as Li_4SiO_4 and $Li_2Si_2O_5$) and Li_2O during initial lithiation can alleviate the volume variation of SiO_x and act as a stable solid-state electrolyte [6, 7]. Unfortunately, the large volume expansion during the lithiation/de-lithiation still exists, which will lead to the pulverization of active material, as well as severely hinder the long cycle lifetime of the SiO_x anodic LIBs [8, 9]. On the other hand, the intrinsic poor electronic conductivity of SiO_x also exerts negative effect on the electrochemical properties [10].

In order to simultaneously address the issues, some of the following effective strategies have been developed for suppressing the volume expansion effect of SiO_x and enhancing its conductivity: 1) Reducing the size of SiO_x to nanoscle can efficiently alleviate volume expansion and shorten the transport distance of ions and electrons; and 2) designing composite material, especially combining SiO_x with carbon and conductive polymer to enhance the conductivity [11–14]. For example, Mai et al. [13] reported a unique yolk@shell structured SiO_x/C composite through sol–gel method and selective etching. The yolk@shell structures with carefully engineered void space have been demonstrated to be quite effective for addressing the issue of volume changes. However, complicated processes restrict its application. Mu et al. [15] combined the Stöber method and spary drying to synthesize SiO_2/MXene microspheres. The flexible MXene matrix could efficiently relieve the strain induced by large volume variation of SiO_2 upon cycling. Meanwhile, MXene could provide conductive networks to promote the transfer of electrons and diffusion of lithium ions. However, it is still urgent to develop facile method to obtain specific SiO_x nanostructures with low cost and controllable regulations.

Since the first discovery of graphene in 2004, two-dimensional (2D) materials have been widely studied owing to their ultra-thin structure and unique photoelectric properties [16–20]. Due to its unique 2D structure, SiO_x nanosheets are regarded as potential anode materials for lithium batteries, which can effectively alleviate the huge volume expansion of SiO_x during charging and discharging. $CaSi_2$ is a layered Zintl compound in which the Ca and Si atomic layers are alternately stacked. Developing practical methods to exfoliate $CaSi_2$ is considered as a hopeful route for the facile access to 2D Si nanomaterials. The synthesis methods of 2D Si based nanosheets from $CaSi_2$ mainly include wet chemical stripping method and

Address correspondence to Lin Sun, chem_sun@ycit.edu.cn; Ruoyu Chen, chry@cczu.edu.cn; Zhong Jin, zhongjin@nju.edu.cn

solvothermal method, etc. [21–23]. Our group previously [21] employed a solvothermal method to obtain SiO_x nanosheets from $CaSi_2$ in ionic liquid circumstances, but concurrently comprising cumbersome steps and low yield. Overall, the existing preparation methods have complicated processes and insufficient stripping, and require high temperature or multi-step treatment to coat carbon or other metal particles. Therefore, it is crucial to develop a one-step carbon or metal coating method.

In this work, we developed a facile one-pot complex redox reaction method or the synthesis of SiO_x/C-Ag composite nanosheets. In this design, the Si_6H_6 nanoplates derived from Zintl phase $CaSi_2$ can steady react with $AgNO_3$-aniline complex. Specifically, aniline served as carbon sources, and Si_6H_6 could be oxdized to SiO_x by $AgNO_3$ in mild solution condition. It should be indicated that, the byproduct AgCl will be easily produced in the absence of aniline. When served as anodes in LIBs, the obtained SiO_x/C-Ag nanocomposite possesses some merits. Firstly, 2D structures can accelerate lithium ion and electron diffusion and mitigate the volume changes. In addition, the coated carbon layer derived from the pyrolysis of aniline can act as conductive skeletons and provide migration paths for electrons, which can improve the overall performance of SiO_x based anodes.

2 Experimental details

2.1 Chemicals

$CaSi_2$ was purchased from Alfa Aesar, and the other reagents were purchased from Sinopharm Chemical Reagent Co., Ltd., and acetonitrile was dried over zeolite.

2.2 Preparation of Si_6H_6

Si_6H_6 was prepared according to reported literature [24]. 4 g $CaSi_2$ was slowly added to 400 mL of concentrated HCl, and then stirred at −30 °C under the protection of the nitrogen atmosphere for 5 days. Si_6H_6 was collected by centrifugation, washed with acetonitrile several times and dried at 60 °C for 6 h under vacuum.

2.3 Preparation of SiO_x/C-Ag nanosheets

Under the protection of the nitrogen atmosphere, 0.6 g Si_6H_6 was dispersed in 120 mL acetonitrile under ultrasonication for 30 min. After that, 220 μL aniline solution contained $AgNO_3$ (180 mg $AgNO_3$ was dissolved in 540 μL aniline) was slowly added, and the mixture was further stirred for 20 h at 50 °C. Next, a yellow powder was obtained by removing the acetonitrile solvent by rotary evaporation. The residue was calcined in a tube furnace at 650 °C under argon atmosphere for 5 h to produce SiO_x/C-Ag composite material.

2.4 Characterizations

Powder X-ray diffraction (PXRD) data was collected on a X'Pert3 powder diffractometer system using Cu Kα radiation at room temperature with 2θ range from 5 to 90°. scanning electron microscopy (SEM) images and energy dispersive spectroscopy (EDS) were obtained on a Nova NanoSEM 450 (USA) field emission scanning electron microscope with acceleration voltages of 5.0 and 10.0 kV, respectively. Transmission electron microscopy (TEM) characterization was performed using JEM-2100F (Japan). X-ray photoelectron spectroscopy (XPS) measurements were recorded with ESCALAB 250Xi. Fourier transform infrared (FTIR) spectroscopy was measured on the FTIR spectrometer (NEXUF-670) using KBr particle method. Under an air atmosphere, thermogravimetric (TG) analysis was performed on a STA 449C3/G (Germany) thermal analyzer. Raman spectroscopy (LabRAM HR Evolution, Horiba, equipped with a 633 nm laser) was used to study the structure of SiO_x/C-Ag nanosheets.

2.5 Electrochemical measurements

The electrochemical performance of SiO_x/C-Ag as the anode material of LIBs was studied by using 2025 button battery components (where pure Li foil was used as the counter electrode). The CR2025 battery was assembled in a glove box filled with argon gas (both H_2O and O_2 < 0.1 ppm). A mixture of 80 wt.% active ingredient, 10 wt.% conductive graphite, and 10 wt.% sodium carboxymethyl cellulose (CMC) was mixed using agate mortar and stirred in water and the formed mash was coated on a Cu foil with a spatula. After vacuum drying at 100 °C for 10 h, the foil was cut into discs with a diameter of 14 mm. The total mass load of active substance on the electrode was about 1 mg·cm^{-2}. The electrolyte consisted of a solution of 1 M $LiPF_6$ in a mixture of 1: 1 (v/v) ethylene carbonate/diethyl carbonate and 2 wt.% vinylene carbonates (Dado Chemical Reagent, China). The measurement was performed on the Neware battery test equipment (Shenzhen, China) in a constant current mode with a charge–discharge cycle voltage of 0.01–3 V. The specific capacity was calculated based on the total mass of the active material. The cyclic voltammogram (CV) was recorded on an electrochemical workstation (CHI660E, Chenhua, CHN) with a scan rate of 0.2 mV·s^{-1} and a range of 0 to 3.0 V. Electrochemical impedance spectroscopy (EIS) was performed from 100 kHz to 0.01 Hz over the entire frequency range. The whole process of battery test was carried out at 28 °C.

3 Results and discussion

Figure 1 exhibits the preparation process of SiO_x/C-Ag. Firstly, the hydrogen passivated Si (Si_6H_6) nanosheets were obtained via concentrated HCl exfoliation method under low temperature. Afterwards, $AgNO_3$ was employed as oxidizing agent. It should be noted that the intinsic oxidizability of $AgNO_3$ was strong enough to directly transform Si^{-1} into Si^0. However, due to the presence of chloride ions in Si_6H_6 (the residual chloride ion was hardly removed via washing), the direct reaction between Si_6H_6 and $AgNO_3$ would effortless to form AgCl byproduct (Fig. S1 in the Electronic Supplementary Material (ESM)). In order to avoid the side reaction, we innovatively utilized a complex redox reaction to realize the facile synthesis of SiO_x/C-Ag nanosheets. Here, aniline was selected as a complexing agent to bind Ag^+ and concurrently served as the carbon source.

Figure S2 in the ESM shows the SEM image of bulk $CaSi_2$, which composed of irregular particles. At first, the commercial

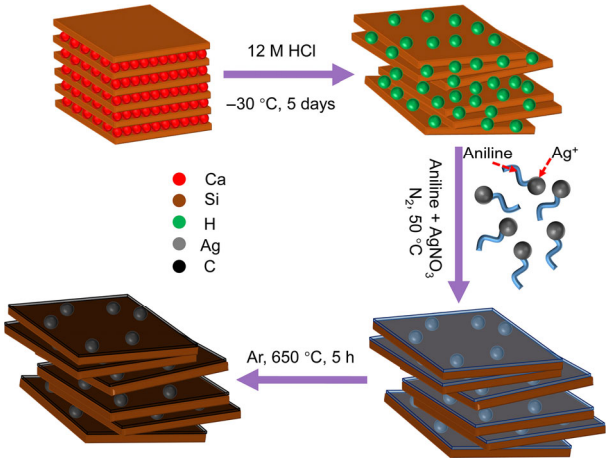

Figure 1 Schematic illustration of the preparation of SiO_x/C-Ag.

$CaSi_2$ was rinsed with 2 M NaOH aqueous solution to remove as-received Si impurity (Fig. S1 in the ESM). After etching with concentrated HCl, the calcium layer was removed to form the swollen stacking layers as shown in Fig. 2(a). TEM image of the as-prepared SiO_x/C-Ag nanosheets (Fig. 2(b)) shows the multi-layered structure and the modified Ag nanoparticles. Figure 2(c) clearly shows the Ag nanoparticle with diameter of ~ 30 nm and the presence of partially graphited carbon. Figure 2(d) shows high-resolution TEM (HRTEM) image of SiO_x/C-Ag nanosheets, one set of lattice fringes with 0.22 nm can be indexed to (111) crystal plane of the Ag phase. In addition, Raman spectroscopy (Fig. 3(b)) of the SiO_x/C-Ag nanosheets also demostrates the exsistence of carbon, the calculated I_D/I_G ratio for the SiO_x/C-Ag is about 1.5, suggesting that the carbon layer of the nanocomposite is amorphous. Moreover, SEM image and the corresponding elemental mapping were performed to further confirm the elemental distribution in the composite (Figs 2(e)–2(g)). The coated carbon was estimated to be ~ 2 wt.% by TG analysis (Fig. S3 in the ESM), which indicated that redox reaction played an important role in the formation of SiO_x-carbon nanocomposites.

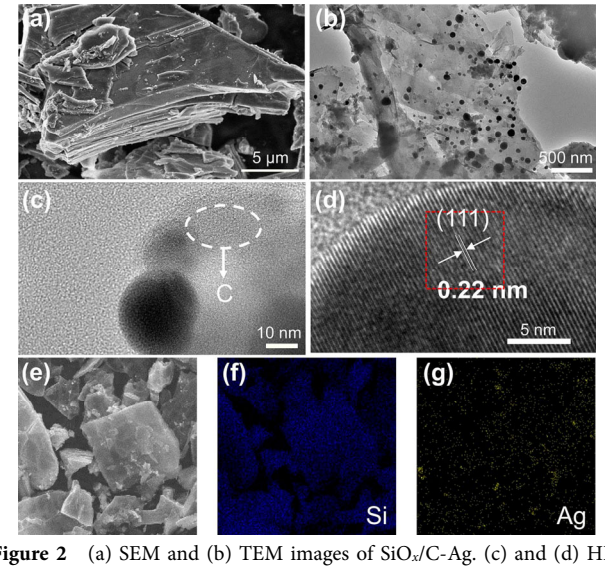

Figure 2 (a) SEM and (b) TEM images of SiO_x/C-Ag. (c) and (d) HR-TEM images of SiO_x/C-Ag. (e)–(g) SEM image and elemental mapping of SiO_x/C-Ag.

PXRD technique was further carried out to confirm the structures of as-prepared samples. The green line of Si_6H_6 in Fig. 3(a) shows only a broad peak located at around 25° [25], with no silicon contaminants after rinsing with 2 M NaOH aqueous solution. After calcining, the peak located at 25° shifted to the left as shown in the red line of SiO_x/Ag-C in Fig. 3(a), which indicates the valence state of Si is change. The FTIR spectra of the obtained Si_6H_6 nanosheets (the green line in Fig. S4 in the ESM) show peaks at 2,112 and 609 cm^{-1}, which can be attributed to the Si–H stretching vibrations for Si_6H_6 [26]. After reacted with $AgNO_3$-aniline complex, the characteristic of the Si-H stretching vibrations was disappeared, as illustrated in the red line in the Fig. S4 in ESM. In addition, there is a strong and broad absorption peak at 1,096 cm^{-1} due to the Si–O–Si anti-symmetric stretching vibration, indicating that the obtained nanosheets were oxidized. Meanwhile, the peaks at 3,400 and 863 cm^{-1} can be assigned to the –OH and Si–OH stretching vibrations, respectively. The peaks at 805 and 494 cm^{-1} are originated from Si-O symmetric stretching vibration. The PXRD pattern of the SiO_x/C-Ag nanosheets show five diffraction peaks located at 38.1, 44.2, 64.4, 77.4, and 81.5°, which are assigned to the (111), (200), (220), (311), and (222) crystal planes of the Ag phase (PDF#: 04-0783) [27]. In addition, it also shows a broad peak located at around 22°, which is assigned to SiO_x [28]. Moreover, The strong and broad absorption peak at 1,096 cm^{-1} is due to the Si–O stretching vibration [21], indicating that the obtained nanosheets were partially oxidized. The as-prepared composites were further characterized by XPS. Figure 3(c) shows that the SiO_x/C-Ag sample has five characteristic peaks corresponding to Si 2p, Ag 3d, C 1s, N 1s, and O 1s. As we know, Si is easily oxidized to oxides during the synthesis process. As shown in Fig. 3(d), the Si 2p spectrum can be deconvolved into three peaks at 102.9, 103.6, and 104.5 eV, which corresponded to Si (+2), Si (+3), and Si (+4) species, respectively [29]. The Ag 3d spectrum (Fig. 3(e)) shows two peaks of Ag species: Ag $3d_{3/2}$ (374.2 eV) and Ag $3d_{5/2}$ (368.2 eV) [30]. As expected, the Ag 3d XPS spectrum indicates that Ag exists in the form of Ag^0. After five cycles at the current density of 0.1 $A{\cdot}g^{-1}$, the Ag 3d spectrum (Fig. S5 in the ESM) indicates that the valence state of Ag was not changed, which means the modified Ag nanoparticles in 2D SiO_x/C nanosheets maintain well before and after cycling. In addition, the PXRD pattern of SiO_x/Ag-C andoes (Fig. S6 in the

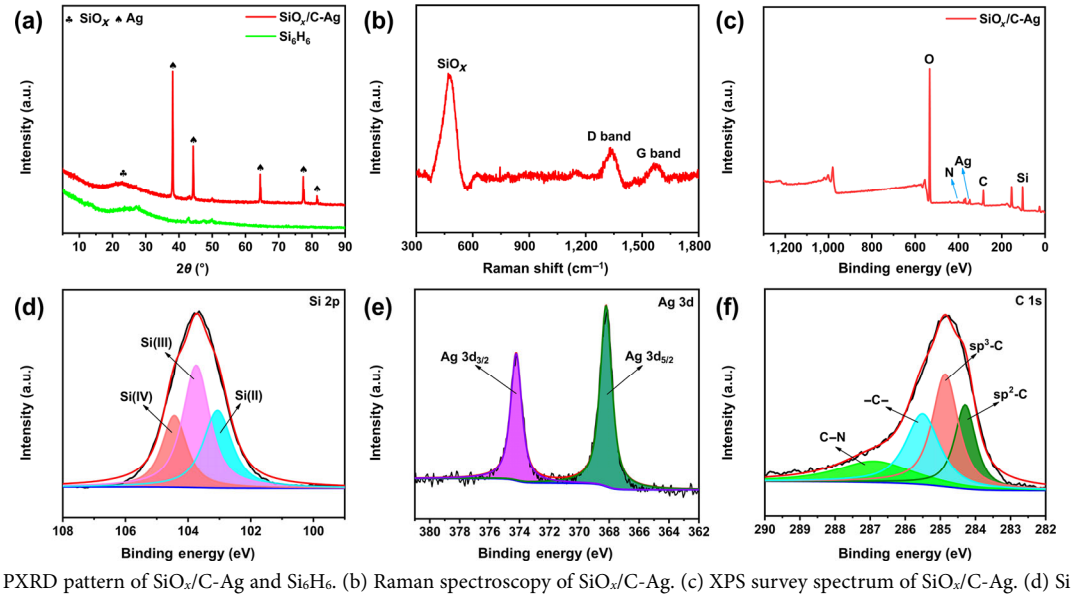

Figure 3 (a) PXRD pattern of SiO_x/C-Ag and Si_6H_6. (b) Raman spectroscopy of SiO_x/C-Ag. (c) XPS survey spectrum of SiO_x/C-Ag. (d) Si 2p, (e) Ag 3d, and (f) C 1s XPS spectra of SiO_x/C-Ag, respectively.

ESM) that after several charge–discharge cycles also confirms the existence of Ag^0 without changes. The C 1s spectrum (Fig. 3(f)) can be deconvoluted into four peaks: sp^2-C (284.28 eV), sp^3-C (284.85 eV), the hetero-carbon bond (285.5 eV), and the carbon bond directly connected to nitrogen (286.8 eV) [31]. The EDS spectrum of SiO_x/C-Ag, which is shown in Fig. S7 in the ESM, also demonstrates the existence of carbon and Ag nanoparticle. After charging–discharging for 500 cycles, the Ag also exists in the electrode and has not disappeared, as illustrated in Fig. S8 in the ESM. The weight ratio of Si and Ag is 10.98 wt.%, and atomic ratio of Si and Ag is 42.4 at.%, which is consistent with XPS analysis. Although chlorine element can be detected, it seems like adhered to the SiO_x nanosheets surface and exists in the form of chloride ions, rather than AgCl byproduct. It can be clearly seen from Fig. S1 in the ESM that the comple-redox reaction avoids the formation of AgCl [32], which further proves the presence of silver nanoparticles in the product.

The electrochemical performance of the SiO_x/C-Ag electrode was evaluated and shown in Fig. 4. The lithiation/de-lithiation properties of the electrode were evaluated by CV in the voltage range of 0.01–3 V (vs. Li/Li^+) with a scan rate of 0.01 $mV·s^{-1}$, as shown in Fig. 4(a). For SiO_x/C-Ag electrode, two distinct peaks at 1.2 and 0.7 V during the first cathodic scan are attributed to the formation of the solid electrolyte interfaces (SEI) film [33]. Another two distinct peaks at 0.25 and 0.5 V during the three cathodic scans represent de-lithium process. The second and third cycle almost overlap, which shows the good reversibility of the sample [33]. In addition, a noticeable broad reduction peak at around 0.5 V in the next cycles is due to the intercalated-Li potential, and an anodic peak is located at around 0.3 V, attributing to the de-lithium of the Li-SiO_x alloys[33].

Figure 4(b) shows the first three charge–discharge curves in the voltage window of 0.01–3 V (vs. Li/Li^+) at a current density of 0.1 $A·g^{-1}$. In the first discharging process, the plateau at around 0.7 V is assigned to the formation of the SEI film. A long voltage plateau between 0.01 and 0.2 V is attributed to the full lithiation of SiO_x/C-Ag. The charging plateau at around 0.5 V is ascribed to the full de-lithiation of the SiO_x/C-Ag electrode. The specific discharge capacity reaches as high as 1,477 $mAh·g^{-1}$, while the first specific charge capacity is 966 $mAh·g^{-1}$, endowing the first cycle Coulombic efficiency (C.E.) is 65.4%. The irreversible capacity of the first cycle may be due to the irreversible formation of SEI film. In the second and third charge/discharge process, the charge/discharge curves tend to be stable, with a C.E. of about 90%. In the next cycles, the C.E. Values increase and remain nearly about 100%.

Figure 4(c) shows the rate performance of SiO_x/C-Ag, which was studied by the Neware battery test equipment in the voltage range of 0.01–3 V (vs. Li/Li^+) with different current densities. After five cycles at the current density of 0.1 $A·g^{-1}$, the SiO_x/C-Ag electrode shows discharge capacity of 800 $mAh·g^{-1}$. Although in the big current density of 2.4 and 4.8 $A·g^{-1}$, the sample also has discharge capacities of 280 and 160 $mAh·g^{-1}$, and with return to the initial current density of 0.1 $A·g^{-1}$, it also has 800 $mAh·g^{-1}$ approximately. The significantly excellent rate performance of the SiO_x/C-Ag nanosheets mainly benefits from the uniform structure and the incorporation of graphite carbon cloth, which leads to a significant increase of the electron transportation path within the nanohybrid [34].

The cyclic stability of SiO_x/C-Ag nanosheets electrode was performed at a current density of 0.6 $A·g^{-1}$ with the voltage window between 0.01 and 3.0 V (vs. Li/Li^+). As shown in Fig. 4(d), the electrode exhibits steady capacity increasement in first dozens of cycles due to the electrode activation. After charging/discharging for 500 times, the SiO_x/C-Ag nanosheets (Fig. 4(d)) electrode still holds specific capacity of 550 $mAh·g^{-1}$ and Coulombic efficiency is maintained at a constant of about 100%. For comparison, at the current density of 0.5 $A·g^{-1}$, the SiO_x nanosheets (Fig. S9 in the ESM) electrode merely maintains the capacity of ~71 $mAh·g^{-1}$ after 500 cycles, which is far lower than that of SiO_x/C-Ag electrode. It is mainly attributed to the coated thin carbon layer. In addition, at the current density of 1 $A·g^{-1}$, the SiO_x/C-Ag nanosheets electrode (Fig. S10 in the ESM) still maintains the capacity of ~ 300 $mAh·g^{-1}$ after 24 cycles. As shown in Table S1 in the ESM, it is found that the specific capacity of our SiO_x/C-Ag electrode is competitive when compared with some reported SiO_2 or SiO_x electrodes. Specifically, the reversible specific capacity of SiO_x/C-Ag electrode reaches as high as ~ 800 $mAh·g^{-1}$ when cycling at the current density of 0.1 $A·g^{-1}$, as shown in Fig. S11 in the ESM. Figure S12 in the ESM shows the EIS of the SiO_x/C-Ag nanosheets, which confirms the improvement of the electrochemical performance after carbon coating. While the SEM

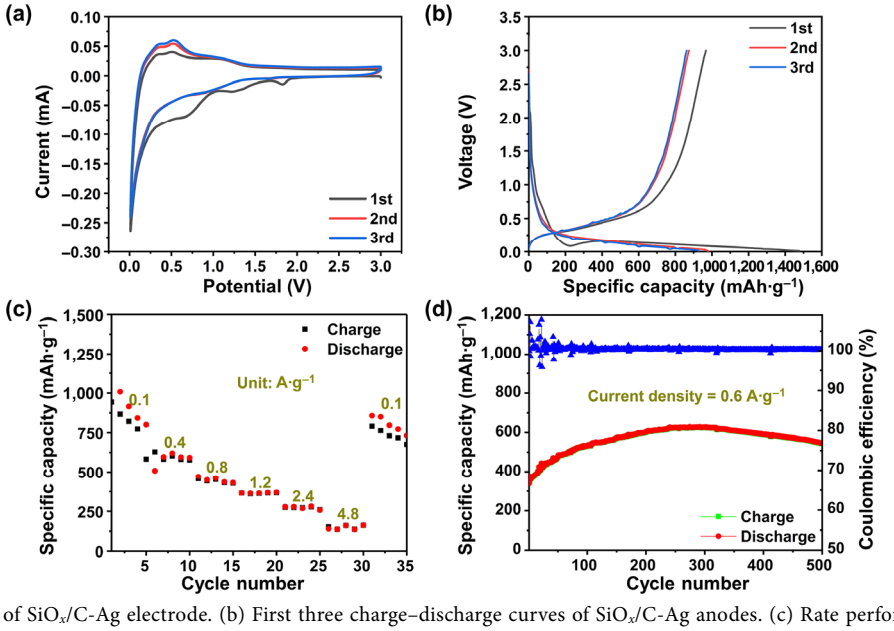

Figure 4 (a) CV curve of SiO_x/C-Ag electrode. (b) First three charge–discharge curves of SiO_x/C-Ag anodes. (c) Rate performance and (d) cycling stability of SiO_x/C-Ag anodes.

images of SiO_x/C-Ag nanosheets electrode bafore and after cycling for 500 times are shown in Fig. S13 in the ESM, no obvious cracks or pulverizations can be displayed via comparison between Figs. S13(a) and 13(b) in the ESM, which further illuminates that the 2D SiO_x/C-Ag nanosheets electrode possesses superior electrochemical stability due to the 2D structures and thin carbon coatings. Meanwile, $AgNO_3$ served as an oxidizing agent to transform Si_6H_6 into SiO_x/C in mild solution conditions.

4 Conclusions

In summary, here we proposed a facile complex redox reaction to prepare Ag modified 2D SiO_x/C nanosheets in a batch scale. The 2D Si_6H_6 nanosheets derived from Zintl phase $CaSi_2$ could be steady reacted with $AgNO_3$-aniline complex, Ag ions served as the oxidizing agent to transform Si^{-1} into Si^0, concurrently, the presence of aniline effectively avoided the formation of AgCl byproduct, as well as provided the coated carbon layer on the surface of SiO_x nanosheets. The obtained SiO_x/C-Ag nanosheets electrode exhibited high capacity and excellent cycling stability when serving as anode material in LIBs. The electrode delivered reversible specific capacity as high as ~ 550 $mAh{\cdot}g^{-1}$, and no capacity fading could be observed even after cycing at 0.6 $A{\cdot}g^{-1}$ for 500 times. We expect that this work will provide new insights and inspirations to rationally design and fabricate low-dimensional Si-based anode materials for high-performance LIBs.

Acknowledgements

This work was supported by the National Key Research and Development Program of China (Nos. 2017YFA0208200 and 2016YFB0700600), the Fundamental Research Funds for the Central Universities of China (No. 0205-14380219), the National Natural Science Foundation of China (Nos. 22022505, 51772258, 21872069, and 51761135104), the Natural Science Foundation of Jiangsu Province (Nos. BK20181056, BK20180008, and BK20191042), Jiangsu Postdoctoral Science Fundation (No. 2020Z258), Jiangsu Province Cultivation Base for State Key Laboratory of Photovoltaic Science and Technology (No. SKLPST201901), and Funding for school-level research projects of Yancheng Institute of Technology (No. xjr2019006).

Electronic Supplementary Material: Supplementary material (PXRD patterns, SEM images, TG curve, FITR spectra, XPS survey, EDS spectra, EIS curves, and electrochemical performance) is available in the online version of this article at https://doi.org/10.1007/s12274-021-3491-z.

References

[1] Yoshino, A. The birth of the lithium-ion battery. *Angew. Chem., Int. Ed.* **2012**, *51*, 5798–5800.

[2] Ritchie, A. G. Recent developments and future prospects for lithium rechargeable batteries. *J. Power Sources* **2001**, *96*, 1–4.

[3] Liu, N.; Huo, K. F.; McDowell, M. T.; Zhao, J.; Cui, Y. Rice husks as a sustainable source of nanostructured silicon for high performance Li-ion battery anodes. *Sci. Rep.* **2013**, *3*, 1919.

[4] Chang, W. S.; Park, C. M.; Kim, J. H.; Kim, Y. U.; Jeong, G.; Sohn, H. J. Quartz (SiO_2): A new energy storage anode material for Li-ion batteries. *Energy Environ. Sci.* **2012**, *5*, 6895–6899.

[5] Cui, J. L.; Cui, Y. F.; Li, S. H.; Sun, H. L.; Wen, Z. S.; Sun, J. C. Microsized porous SiO_x@C composites synthesized through aluminothermic reduction from rice husks and used as anode for lithium-ion batteries. *ACS Appl. Mater. Interfaces* **2016**, *8*, 30239–30247.

[6] Liu, H. K.; Guo, Z. P.; Wang, J. Z.; Konstantinov, K. Si-based anode materials for lithium rechargeable batteries. *J. Mater. Chem.* **2010**, *20*, 10055–10057.

[7] Ban, C. M.; Kappes, B. B.; Xu, Q.; Engtrakul, C.; Ciobanu, C. V.; Dillon, A. C.; Zhao, Y. F. Lithiation of silica through partial reduction. *Appl. Phys. Lett.* **2012**, *100*, 243905.

[8] Liang, Y. R.; Cai, L. F.; Chen, L. Y.; Lin, X. D.; Fu, R. W.; Zhang, M. Q.; Wu, D. C. Silica nanonetwork confined in nitrogen-doped ordered mesoporous carbon framework for high-performance lithium-ion battery anodes. *Nanoscale* **2015**, *7*, 3971–3975.

[9] Cao, X.; Chuan, X. Y.; Massé, R. C.; Huang, D. B.; Li, S.; Cao, G. Z. A three layer design with mesoporous silica encapsulated by a carbon core and shell for high energy lithium ion battery anodes. *J. Mater. Chem. A* **2015**, *3*, 22739–22749.

[10] Zhu, M. Y.; Shen, Y. B.; Chang, L. M.; Yin, D. M.; Cheng, Y.; Wang, L. M. Enabling high electrochemical activity of a hollow SiO_2 anode by decorating it with ultrafine cobalt nanoparticles and a carbon matrix for long-lifespan lithium ion batteries. *Nanoscale* **2020**, *12*, 13442–13449.

[11] Tu, J. G.; Yuan, Y.; Zhan, P.; Jiao, H. D.; Wang, X. D.; Zhu, H. M.; Jiao, S. Q. Straightforward approach toward SiO_2 nanospheres and their superior lithium storage performance. *J. Phys. Chem. C* **2014**, *118*, 7357–7362.

[12] Yu, Q.; Ge, P. P.; Liu, Z. H.; Xu, M.; Yang, W.; Zhou, L.; Zhao, D. Y.; Mai, L. Q. Ultrafine SiO_x/C nanospheres and their pomegranate-like assemblies for high-performance lithium storage. *J. Mater. Chem. A* **2018**, *6*, 14903–14909.

[13] Liu, Z. H.; Zhao, Y. L.; He, R. H.; Luo, W.; Meng, J. S.; Yu, Q.; Zhao, D. Y.; Zhou, L.; Mai, L. Q. Yolk@Shell SiO_x/C microspheres with semi-graphitic carbon coating on the exterior and interior surfaces for durable lithium storage. *Energy Storage Mater.* **2019**, *19*, 299–305.

[14] Ouyang, P. H.; Jin, C. X.; Xu, G. J.; Yang, X. X.; Kong, K. J.; Liu, B. B.; Dan, J. L.; Chen, J.; Yue, Z. H.; Li, X. M. et al. Lithium ion batteries with enhanced electrochemical performance by using carbon-coated SiO_x/Ag composites as anode material. *Ceram. Int.* **2021**, *47*, 1086–1094.

[15] Mu, G.; Mu, D. B.; Wu, B. R.; Ma, C. W.; Bi, J. Y.; Zhang, L.; Yang, H.; Wu, F. Microsphere-like SiO_2/MXene hybrid material enabling high performance anode for lithium ion batteries. *Small* **2020**, *16*, 1905430.

[16] Huang, K.; Liu, G. P.; Lou, Y. Y.; Dong, Z. Y.; Shen, J.; Jin, W. Q. A graphene oxide membrane with highly selective molecular separation of aqueous organic solution. *Angew. Chem., Int. Ed.* **2014**, *53*, 6929– 6932.

[17] Tang, H. J.; Wang, J. Y.; Yin, H. J.; Zhao, H. J.; Wang, D.; Tang, Z. Y. Growth of polypyrrole ultrathin films on MoS_2 monolayers as high-performance supercapacitor electrodes. *Adv. Mater.* **2015**, *27*, 1117–1123.

[18] Li, P. H.; Yang, Y.; Gong, S.; Lv, F.; Wang, W.; Li, Y. J.; Luo, M. C.; Xing, Y.; Wang, Q.; Guo, S. J. Co-doped 1T-MoS_2 nanosheets embedded in N, S-doped carbon nanobowls for high-rate and ultra-stable sodium-ion batteries. *Nano Res.* **2019**, *12*, 2218–2223.

[19] Zhao, X. W.; Wu, Y. Z.; Wang, Y. S.; Wu, H. S.; Yang, Y. W.; Wang, Z. P.; Dai, L. X.; Shang, Y. Y.; Cao, A. Y. High-performance Li-ion batteries based on graphene quantum dot wrapped carbon nanotube hybrid anodes. *Nano Res.* **2020**, *13*, 1044–1052.

[20] Mao, E. Y.; Wang, W. Y.; Wan, M. T.; Wang, L.; He, X. M.; Sun, Y. M. Confining ultrafine Li_3P nanoclusters in porous carbon for high-performance lithium-ion battery anode. *Nano Res.* **2020**, *13*, 1122–1126.

[21] Sun, L.; Su, T. T.; Xu, L.; Liu, M. P.; Du, H. B. Two-dimensional ultra-thin SiO_x ($0 < x < 2$) nanosheets with long-term cycling stability as lithium ion battery anodes. *Chem. Commun.* **2016**, *52*, 4341–4344.

[22] Lin, H.; Qiu, W. J.; Liu, J. J.; Yu, L. D.; Gao, S. S.; Yao, H. L.; Chen, Y.; Shi, J. L. Silicene: Wet-chemical exfoliation synthesis and biodegradable tumor nanomedicine. *Adv. Mater.* **2019**, *31*, 1903013.

[23] De Crescenzi, M.; Berbezier, I.; Scarselli, M.; Castrucci, P.; Abbarchi, M.; Ronda, A.; Jardali, F.; Park, J.; Vach, H. Formation of silicene nanosheets on graphite. *ACS Nano* **2016**, *10*, 11163–11171.

[24] Dahn, J. R.; Way, B. M.; Fuller, E.; Tse, J. S. Structure of siloxene and layered polysilane (Si_6H_6). *Phys. Rev. B* **1993**, *48*, 17872–17877.

[25] Kumai, Y.; Kadoura, H.; Sudo, E.; Iwaki, M.; Okamoto, H.; Sugiyama, Y.; Nakano, H. Si–C composite anode of layered polysilane (Si_6H_6) and sucrose for lithium ion rechargeable batteries. *J. Mater. Chem.* **2011**, *21*, 11941–11946.

[26] Pazhamalai, P.; Krishnamoorthy, K.; Sahoo, S.; Mariappan, V. K.; Kim, S. J. Understanding the thermal treatment effect of two-dimensional siloxene sheets and the origin of superior electrochemical energy storage performances. *ACS Appl. Mater. Interfaces* **2019**, *11*, 624–633.

[27] Majeed Khan, M. A.; Kumar, S.; Ahamed, M.; Alrokayan, S. A.; AlSalhi, M. S. Structural and thermal studies of silver nanoparticles and electrical transport study of their thin films. *Nanoscale Res. Lett.* **2011**, *6*, 434.

[28] Nakano, H.; Ishii, M.; Nakamura, H. Preparation and structure of novel siloxene nanosheets. *Chem. Commun.* **2005**, 23, 2945–2947.

[29] Xiang, X. M.; Zhao, H. H.; Yang, J.; Zhao, J.; Yan, L.; Song, H. L.; Chou, L. J. Nickel based mesoporous silica-ceria-zirconia composite for carbon dioxide reforming of methane. *Appl. Catal. A* **2016**, *520*, 140–150.

[30] Li, K.; Cui, S. S.; Hu, J. L.; Zhou, Y. F.; Liu, Y. C. Crosslinked pectin nanofibers with well-dispersed Ag nanoparticles: Preparation and characterization. *Carbohydr. Polym.* **2018**, *199*, 68–74.

[31] Lesiak, B.; Kövér, L.; Tóth, J.; Zemek, J.; Jiricek, P.; Kromka, A.; Rangam, N. C sp^2/sp^3 hybridisations in carbon nanomaterials-XPS and (X)AES study. *Appl. Surf. Sci.* **2018**, *452*, 223–231.

[32] Xu, Y. G.; Xu, H.; Li, H. M.; Xia, J. X.; Liu, C. T.; Liu, L. Enhanced photocatalytic activity of new photocatalyst Ag/AgCl/ZnO. *J. Alloys Compd.* **2011**, *509*, 3286–3292.

[33] Zhang, L.; Deng, J. W.; Liu, L. F.; Si, W. P.; Oswald, S.; Xi, L. X.; Kundu, M.; Ma, G. Z.; Gemming, T.; Baunack, S. et al. Hierarchically designed SiO_x/SiO_y bilayer nanomembranes as stable anodes for lithium ion batteries. *Adv. Mater.* **2014**, *26*, 4527–4532.

[34] Zhu, G. J.; Zhang, F. Z.; Li, X. M.; Luo, W.; Li, L.; Zhang, H.; Wang, L. J.; Wang, Y. X.; Jiang, W.; Liu, H. K. et al. Engineering the distribution of carbon in silicon oxide nanospheres at the atomic level for highly stable anodes. *Angew. Chem., Int. Ed.* **2019**, *58*, 6669–6673.